Polymer Testing 82 (2020) 106298

Contents lists available at ScienceDirect

Polymer Testing

journal homepage: http://www.elsevier.com/locate/polytest

Material Performance

In vitro and in vivo evaluation of chitosan-alginate/gentamicin wound dressing nanofibrous with high antibacterial performance

H.R. Bakhsheshi-Rad [a,*], Z. Hadisi [b], A.F. Ismail [c], M. Aziz [c], M. Akbari [b], F. Berto [d], X.B. Chen [e]

[a] Advanced Materials Research Center, Department of Materials Engineering, Najafabad Branch, Islamic Azad University, Najafabad, Iran
[b] Laboratory for Innovations in MicroEngineering (LiME), Department of Mechanical Engineering, University of Victoria, Victoria, BC V8P 5C2, Canada
[c] Advanced Membrane Technology Research Center (AMTEC), Universiti Teknologi Malaysia, 81310, Skudai, Johor Bahru, Johor, Malaysia
[d] Department of Mechanical and Industrial Engineering, Norwegian University of Science and Technology, 7491, Trondheim, Norway
[e] Department of Mechanical Engineering, College of Engineering, University of Saskatchewan, Saskatoon, SK S7N 5A9, Canada

ARTICLE INFO

Keywords:
Chitosan-alginate
Electrospinning
Wound dressings
Antibacterial activity
Biompatibility

ABSTRACT

Wound dressings based on nanofiber polymer scaffolds with good antimicrobial performance and skin reconstruction ability are promising options to thwart wound infection and accelerate wound healing. This paper reports on the synthesis via electrospinning of chitosan-alginate (CS-Alg) nanofiber dressings with various amounts of gentamicin (Gn; 0–10 wt%) as a drug delivery system. Smooth and continuous nanofibers with no obvious beads were created, with increases in the amount of Gn resulting in reduced fiber diameter. Antimicrobial tests showed the Gn-loaded nanofibers had good antibacterial performance as indicated by the inhibition of bacterial growth. CS-Alg nanofibers loaded with higher Gn concentrations exhibited greater antibacterial performance than those with lower Gn concentrations. In vitro cell culture studies demonstrated that CS-Alg wound dressings with 1–3% Gn improved L929 cell attachment and proliferation more than wound dressings with higher Gn concentrations. In vivo experiments revealed that Cs-Alg nanofibers loaded with 3% Gn significantly enhanced skin regeneration in a Balb/C mice model by stimulating the formation of a thicker dermis, increasing collagen deposition, and increasing the formation of new blood vessels and hair follicles. Collectively, Gn-loaded CS-Alg wound dressings can be considered a good candidate for drug delivery systems and skin regeneration applications.

1. Introduction

Wound dressings play an essential function in supporting the healing of particular kinds of wounds [1]. An ideal dressing needs to have certain capabilities, such as supporting a moist environment at the wound interface, permitting gaseous exchange, serving as an obstacle to microorganisms, and eliminating excess exudates [2,3]. Numerous kind of polymers for wound dressing applications have been utilized, including alginate, collagen, and CS in various shapes in the form of films, foams, fibers, or hydrophilic gels [4–7]. Furthermore, among the many varieties of natural polymers for manufacturing wound dressings, CS is regarded as an extremely favorable material because of its outstanding cytocompatibility, nontoxicity, and antibacterial performance [8–11]. In this regard, Huang et al. [12] showed that layer-by-layer nanofibrous mats containing CS could improve biocompatibility and significantly enhanced the skin regeneration. Similarly, Tu et al. [13] conclude that natural polymer containing carboxymethyl chitosan (CMC) materials might be employed as nanofibrous matrices for accelerating wound healing rate, particularly for infected wounds. In other study, Xin et al. [14] showed that using natural biopolymers as coating materials on the surface of nanofibrous mats leads to better cell attachment and proliferation. However, it is not easy to prepare nanofibers from neat CS owing to its cationic charge [3,15]. Several examinations demonstrate that blending polymer [16,17] including CS with other polymers enhances fiber formation and increases its functional characteristics [18]. Alginate (Alg) is a biocompatible polysaccharide that is typically employed in pharmaceutical, cosmetic, and biomedical applications. However, solid dressings consisting of alginate can absorb water and lengthen the wound healing period and may not be effective hemostatic materials, specifically towards large hemorrhages [3, 19–21].

Even though polymers have outstanding cytocompatibility, their

* Corresponding author. Advanced Materials Research Center, Department of Materials Engineering, Najafabad Branch, Islamic Azad University, Najafabad, Iran.
E-mail addresses: rezabakhsheshi@gmail.com, rezabakhsheshi@pmt.iaun.ac.ir (H.R. Bakhsheshi-Rad).

https://doi.org/10.1016/j.polymertesting.2019.106298
Received 12 September 2019; Received in revised form 13 December 2019; Accepted 14 December 2019
Available online 19 December 2019

antibacterial characteristics are unsatisfactory with respect to preventing infections in wounds [22,23]. Therefore, an additional essential requirement for wound dressing materials to shorten the wound healing period is the targeted delivery of drugs to the wound site [24]. Polymers have been applied as drug carriers to create sustained and controlled antibiotic release systems for the prevention of infections [25,26]. In this context, gentamicin (Gn) is employed as a powerful antibiotic for the treatment of numerous bacterial infections because it is effective against a broad variety (Gram-positive and Gram-negative) of bacteria [25,27,28]. Kondaveeti et al. [25,29] demonstrate the addition of Gn into a polyvinyl alcohol-based wound dressing enhances wound healing compared to traditional products due to the possible impact of Gn and subsequent reduced infection of the wound [30–32]. Infections, particularly those induced by drug-resistant pathogens, can cause serious complications to the wound healing process [33–35]; for example, around 33% of bone implants lead to infections that require a second surgery [36]. Karuppuswamy et al. [37] examined the drug release behavior of polycaprolactone (PCL) nanofibers loaded with tetracycline (TC), demonstrating that PCL/TC mats are able to provide constant drug release for 8 d. Rapacz-Kmita et al. [38] considered the antibacterial performance of a montmorillonite-gentamicin system, showing that incorporation of Gn into the montmorillonite matrix leads to destruction of *E. coli* bacteria. Substantial attempts were conducted to the development of nanofibrous mats for skin regeneration utilizing synthetic and natural polymers [1–4]. However, to the best of our knowledge, the Gn drug-loading capacity of CS-Alg in a polymeric nanofiber has not previously been assessed. In addition, there is no report regarding illustration of the exact antibacterial mechanism of Gn-loaded CS-Alg nanofibrous mats for the enhancement of skin reconstruction. Thus, in this work, CS was blended with Alg to fabricate a new type of dressing via the electrospinning method with high antibacterial performance. Electrospinning is an effortless and flexible method suitable for the preparation of continuous polymer fibers ranging in diameter from the micron-to nano-scale [39–41]. Thus this technique has been extensively used to prepare ultrafine, smooth, and continuous nanofibers [41–44]. Among the several types of wound dressings, nanofibers created by means of electrospinning continue to be extensively employed for wound administration and skin tissue engineering [44,45]. Since nanofibers is able to simulate the structure and function of extracellular matrix (ECM) protein fibers of skin tissue and have a porous structure that permits nutrient and gas transport [44–47]. Here, the characteristics of Gn-loaded CS-Alg electrospun mats, such as morphology and antibacterial performance, were evaluated, along with the attachment and proliferation of fibroblasts on the mats. Finally, the wound healing efficiency of an optimized wound dressing was evaluated for partial burn wounds in a Balb/c mouse model, specifically in terms of wound closure rate, skin regeneration, inflammatory response, and deposition of collagen.

2. Experimental procedure

CS with a low molecular weight and degree of deacetylation of 75–85% was obtained from Sigma-Aldrich (St. Louis, MO, USA), along with sodium alginate (SA; brown algae) and gentamicin (Ph. Eur. grade). All other reagents and solvents were of analytical grade. For preparation of the electrospinning solutions, CS was dissolved in 90% acetic acid at 5% w/v for 48 h at ambient temperature to attain a uniform solution. Alg was then dissolved separately in deionized water for 24 h at ambient temperature and then mixed with CS solution with stirring for 24 h (CS: Alg v/v ratio of 1:1). Various amounts of Gn (1, 3, 5, and 10 wt% relative to the weight of CS-Alg) were then dissolved in the as-prepared CS-Alg to create CS-Alg/Gn solutions that were labeled CS-Alg/1Gn, CS-Alg/3Gn, CS-Alg/5Gn, and CS-Alg/10Gn, respectively. The electrospinning (Fanavaran Nano-Meghyas) process was conducted at room temperature, a constant flow rate of 2.50 mL/h, and a voltage of 15 kV. Aluminum foil was placed 20 cm from the needle tip to collect the electrospun fibers. Thereafter, the electrospun nanofibers were cross-linked for 12 h using glutaraldehyde vapors. Fig. 1 is a schematic presentation of this method. For antibacterial assessment, Gram-positive *Staphylococcus aureus* (ATCC 12600) and Gram-negative *Escherichia coli* (ATCC 9637) were employed in diffusion testing, with DOXY used as a control according to Ref. [48]. The antibacterial effect of the samples incorporating different amounts of Gn was determined by evaluating the inhibition area (IA) using ImageJ software. The water uptake capacity of samples was evaluated after immersion in pseudo extracellular fluid (PECF) as simulated wound fluid for 24 h at 37 °C [49]. The amount of water uptake was determined using the following equation:

$$\text{Water Uptake } (\%) = \frac{W_w - W_0}{W_0} \times 100,$$

where W_0 is the weight of pre-weighted mats and W_w is the weight of wet samples after immersion in PECF for 24 h (excess water was wiped off with filter paper).

To assess cell attachment to the fiber layers, an L929 fibroblast cell line at a concentration of 2×10^4 cells/mL was seeded on sterilized CS-Alg/Gn nanofibers [49] and cultured for 3 d, after which the cell scaffold constructs were stained with DAPI (4′,6-diamidino-2-phenylindole) and then subjected to fluorescence image analysis (blue fluorescence in live cells). All specimens were sterilized using ultraviolet (UV) radiation for at least 2 h before the experiment. In addition, the morphology of the attached cells was examined utilizing scanning electron microscopy (SEM). The cell toxicity of the samples was evaluated utilizing the MTT technique, with cells seeded at a concentration of 10^4 cells/mL in a 24-well plate and allowed to grow for various time periods at 37 °C [48]. The entire experiment was performed in at least triplicate to ensure reproducibility of the results. An average of three measurements was considered for each sample. SEM (JEOL JSM-6380LA) was employed to study the morphology of the nanofibers. The sirius red staining method was used to investigate the expression of collagen by L-929 cells cultured on nanofibers [50]. Sirius red solution (0.1%) was prepared in a saturated solution of picric acid (Sigma-Aldrich, USA) for 1 h. The sulfonic acid groups from the anionic part of the dye react with basic groups of collagen to produce red stains.

To study the in vitro release of Gn from the CS-Alg fibers, the nanofiber samples were immersed in phosphate buffered saline (PBS) and incubated at 37 °C. Drug release from biodegradable polymers is determined via diffusion testing because these types of polymers as employed for drug delivery system are degraded via hydrolysis. As water molecules break the chemical bonds along the polymer chain, the physical integrity of the polymer degrades and permits the release of the drug molecules. At various time points, 1-mL subsamples of the PBS solution were taken to determine the amount of released Gn; this subsample volume was replaced with fresh PBS solution. Released Gn was observed using UV spectrophotometry at a wavelength of 345 nm according to Ref. [48].

For the in vivo study, male Balb/c mice (20–25 g) at 6–8 weeks of age were caged individually and provided access to sterile food and water for 1 week before starting the experiments. All procedures were approved by Tehran University Animal Ethics Committee. Partial burn wounds were generated on the shaved back of anesthetized BALB/c mice. Briefly, the mice were anesthetized using ketamine/xylazine by IP injection. Next, a 0.5-cm diameter brass sample was heated to 85 °C for 5 min and placed for 10 s on the disinfected back skin of each mouse. Mice were randomly divided to three groups (n = 5 mice per group), in which each mouse received either a gauze, Cs-Alg, or Cs-Alg/3Gn dressing as a treatment. Images of wounds taken on day 0, 4, and 7 post-injury were used to measure the wound contraction rate. At day 7 post-injury, treated mice were euthanized and skin tissues were harvested for histopathological analysis. The collected tissues were fixed in 10% formalin, dehydrated, and embedded in paraffin wax. The paraffin embedded blocks were subsequently sectioned on slides to a thickness of

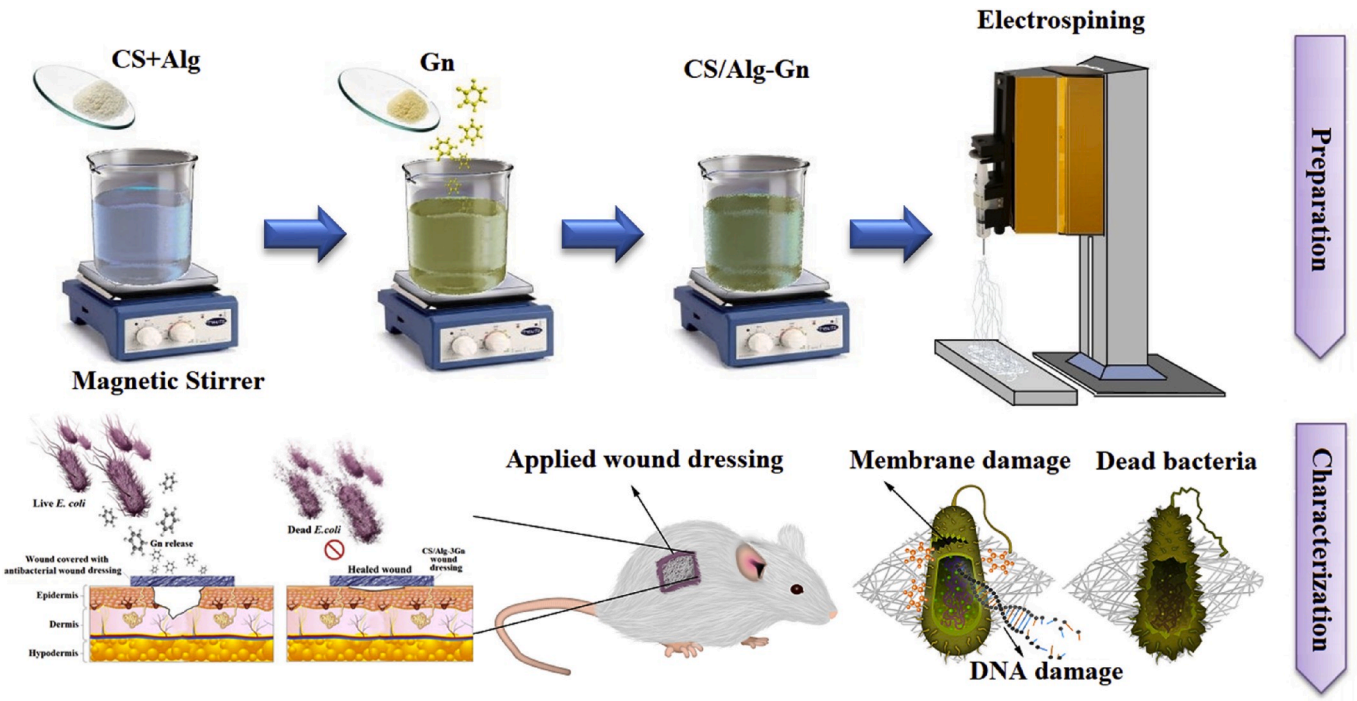

Fig. 1. A schematic representation of the preparation and characterization of CS/Alg-Gn electrospun nanofibers.

5 μm. Finally, hematoxylin and eosin (H&E) and Masson's trichrome (MT) staining were performed according to Ref. [49]. Results are reported as mean ± standard error (SE), analyzed using SigmaPlot software with p values < 0.05 (*) indicating significant differences.

3. Results and discussion

3.1. Fiber characterization

Fig. 2a shows the nanofiber morphology and diameter distribution of the Cs-Alg/xGn mats. The SEM images reveal the smooth and continuous nanofibers with a highly porous structure in the absence of obvious beads achieved via electrospinning. Increasing the Gn content from 1 to 10 wt% leads to an obvious reduction in CS-Alg nanofiber diameter from 398 ± 14 nm (CS-Alg/1Gn) to 301 ± 10 nm (CS-Alg/10Gn) (Fig. 2b). This is likely due to a decline in the viscosity of the electrospinning solution as the Gn concentration increased, resulting in fewer interactions between drug and polymer molecules via hydrogen bonding [37]. In addition, the addition of Gn could increase the number of charge carriers in the polymer solution that often assist in electrospinning, leading to thinner fibers [51]. A histogram analysis (Fig. 2b) shows the wide range of fiber diameters achieved corresponds to that of collagen fibrils (10–300 nm) in native tissue, suggesting these nanofibers could aid in cell growth.

A stress strain curve was generated for the Gn-incorporated CS-Alg nanofibers (Fig. 3a). When employed to aid in the performance of tissue engineering scaffolds, the membranes must be in a position to endure great loads and maintain deformation. With increasing Gn concentration, the tensile strength (Fig. 3b) of the nanofibers increases and subsequently the tensile strain at break decreases (Fig. 3c). Incorporation of 1 and 5 wt% Gn into the CS-Alg nanofibers leads to an incremental increase in tensile strength from 2.91 to 3.35 MPa and increasing tensile strain at break from 33.1 to 38.2%, respectively. Fibers with a smaller diameter are expected to have superior tensile properties and tensile strain. However, incorporation of 10 wt% Gn results in a reduction of both tensile strength and tensile strain to 2.65 MPa and 30.2 wt%,

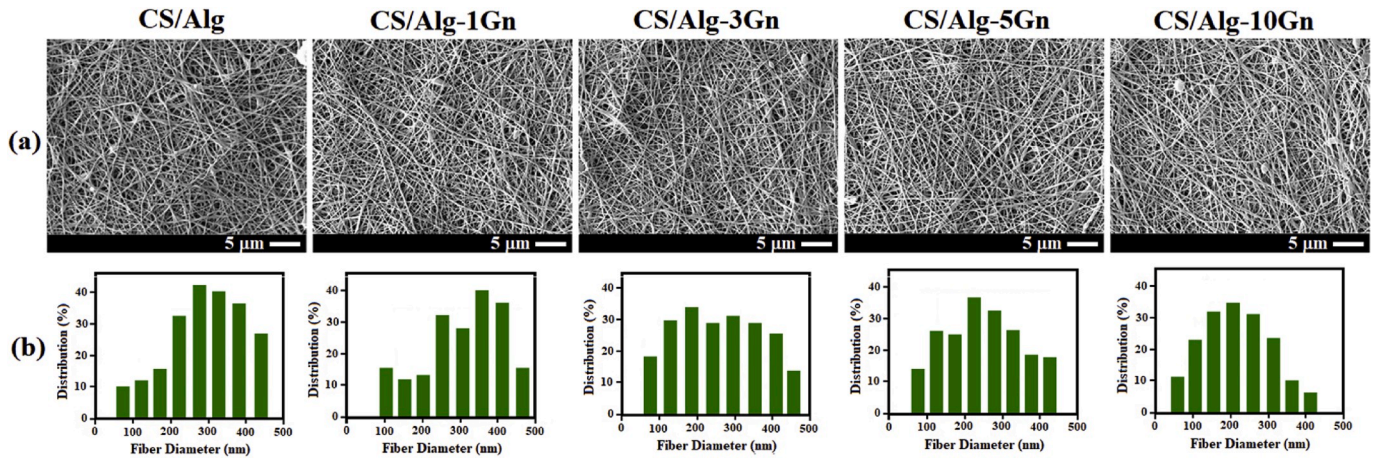

Fig. 2. (a) SEM images and (b) distribution of fiber diameter for CS/Alg-xGn nanofibers (x = 0, 1, 3, 5, and 10 wt%).

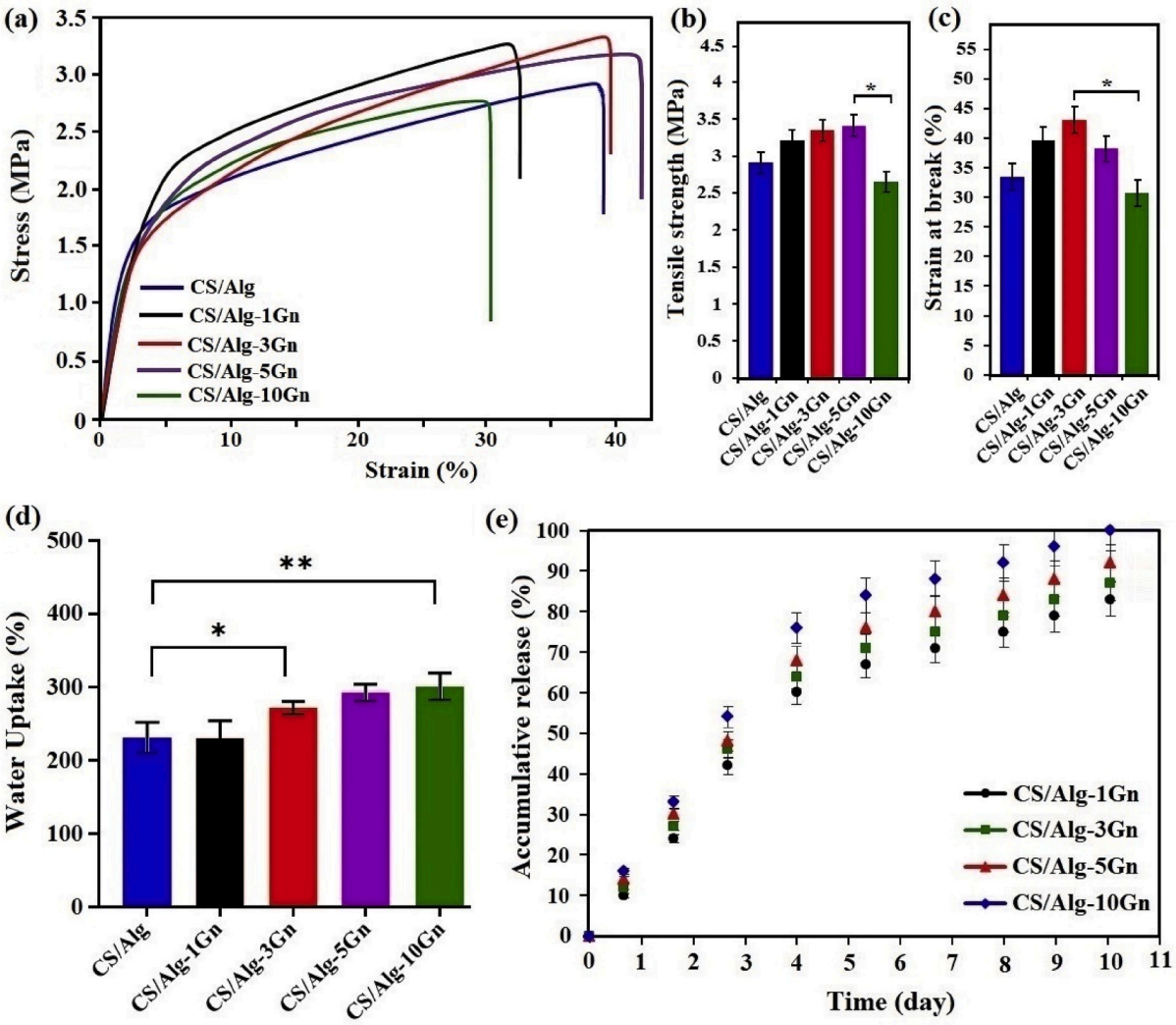

Fig. 3. (a) Stress-strain curves, (b) tensile strength, (c) strain at break, (d) water uptake, and (e) gentamicin release profile of CS/Alg-Gn nanofibers with various Gn concentrations (*p < 0.05, **p < 0.01).

respectively. This is attributed to the structure of the electrospun nanofibers loaded with high concentrations of Gn, which have a rougher structure and large variations in diameter that lead to a reduction in tensile strength [52]. Overall, the CS-Alg nanofibers containing 1–5 wt% Gn have greater tensile strength and higher deformation resistance than those with 0 or 10% Gn.

Wound dressings need to have an appropriate water intake ability to avoid maceration and necrosis of tissue, permit water and nutrient transport, and eliminate wound exudates [53]. Fig. 3d presents changes in the water uptake of the CS-Alg mats with the addition of different concentrations of Gn after soaking in PECF for 24 h. The water absorption capacity of the nanofibers considerably increases with increasing Gn concentration. The CS-Alg mats exhibit the lowest water absorption potential (231.1 ± 8%), but this value climbs (to 295 ± 11%) with increasing Gn content (to 10 wt%). These results might be attributed to the smaller fiber diameter of Gn-incorporated nanofibers, because thinner fibers have a greater specific surface area that results in considerably more water adsorption potential [54]. In addition, decreasing the fiber diameter leads to elevated porosity, which may lead to escalating the water absorption ability of electrospun fibers [55].

3.2. Drug release

Fig. 3e displays the release trend of electrospun fibers loaded with various amounts of Gn. The cumulative release from CS-Alg with 19 wt% Gn features a noticeable burst release of 69.93% within the first 12 h, which is substantially greater than for mats loaded with smaller amounts of Gn. This burst release could be caused by the localization of physically adsorbed drug in the vicinity of the surface, as reported elsewhere [26]. Following this initial burst, a gradual and constant release of Gn is evident until the 10th day, which is probably the longest drug release period for CS-Alg. Despite the fact that the expeditious release of drug at early time points might lessen the infection risk, a gradual release trend is typically more effective [30].

3.3. In vitro cell study

Nanofiber wound dressings that possess a comparable diameter to ECM can facilitate the processes of cell adhesion and proliferation that are essential for skin regeneration [56]. Fig. 4a1-a5 are SEM micrographs of L929 cells cultured on the CS-Alg/Gn nanofibers for 3 d. The cells on the CS-Alg/Gn mats loaded with low concentrations of Gn have a common morphology along with evidence of filopodia that allow the cells to join together; in contrast, cell attachment and proliferation are reduced in the neat CS-Alg mat and dramatically reduced in the CS-Alg mat loaded with a high concentration of Gn. Fluorescence images show cell adhesion on the CS-Alg/Gn nanofibers after 3 d (Fig. 4b1-b5). CS-Alg mats with 1–5 wt% Gn support greater cell adhesion and viability

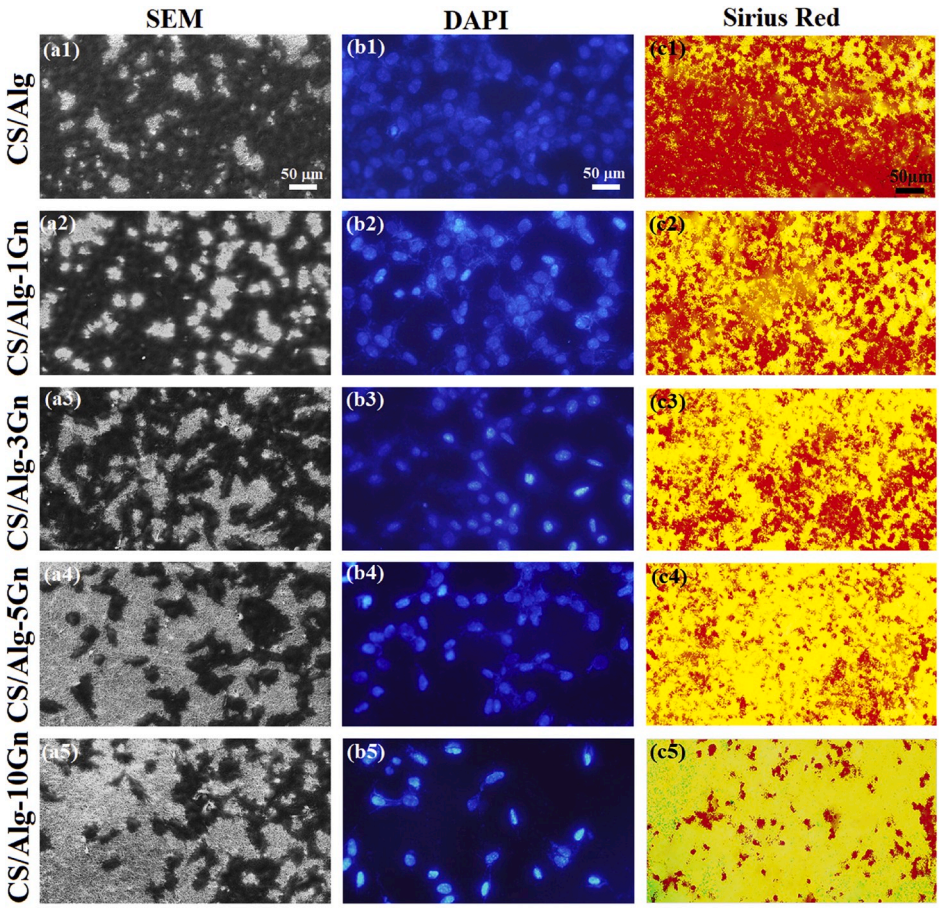

Fig. 4. (a1-a5) SEM images, (b1-b5) DAPI staining, and (c1-c5) sirius red staining of CS/Alg-Gn nanofibers with various Gn concentrations.

than mats with 10 wt% Gn. As such, the incorporation of a minimal concentration of Gn appears to have great potential for enhancing cell viability. The state of wound healing can be determined by measuring the synthesis of ECM, the expression of which by cultured cells is commonly measured by collagen staining with picro-sirius red [57]. Fig. 4c1-c5 depicts the expression of collagen by fibroblasts on CS-Alg/Gn nanofibers after culturing for 7 d. Collagen expression on CS-Alg/Gn nanofibers with lower Gn concentrations is higher than for other samples; in other words, less staining is evident for fibroblasts cultured on Gn-loaded nanofibers with higher Gn content. Furthermore, collagen staining is significantly reduced in CS-Alg/10Gn nanofibers compared to all other nanofibers. As noted above, this may be due to the ability of Gn to stimulate apoptosis in fibroblasts in a dose-dependent manner.

A wound dressing created to make contact with the wound tissue need to have minimal cytotoxicity. The cytotoxicity of CS-Alg/Gn mats toward L929 cells after culturing for 3 and 7 d is displayed in Fig. 5. Plain CS-Alg nanofibers exhibit no noticeable cytotoxicity to the L-929 cell line throughout the period examined, while dose-dependent cytotoxicity to L-929 cells is observed for Gn-loaded CS-Alg nanofibers. In comparison, CS-Alg/10Gn mats have considerably diminished cell viability. Notably, the cell viability of CS-Alg/Gn extracts diminishes with increasing culture time (from 3 to 7 d), which might be attributed to the further release of Gn. These effects are most likely mainly due to the greater amounts of antibiotics released, inducing apoptosis in cells by means of cell membrane destruction and causing stress in the cells by disturbing cell metabolic action [30].

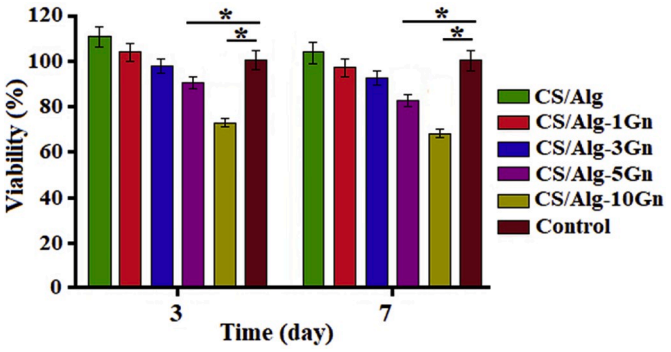

Fig. 5. Cell viability of CS/Alg-Gn nanofibers with various Gn concentrations (*$p < 0.05$).

3.4. Antibacterial study

Two tests were performed to evaluate the antibiotic effectiveness of the fabricated CS-Alg/Gn nanofibers towards *S. aureus* and *E. coli*. In the agar disk diffusion test (Fig. 6a and b), a less significant inhibition zone is noted for the CS-Alg mats without Gn, indicating CS-Alg has minimal anti-bacterial performance. In contrast, the Gn-loaded mats effectively inhibited the growth of bacterial cells throughout the examined incubation time. The scaffolds with a greater concentration of Gn have larger inhibition zones, with the largest towards both *E. coli* and *S. aureus* for the CS-Alg/10Gn scaffolds. Fig. 6c illustrates the percent bacterial inhibition for all samples at various incubation time points. Similar to the diffusion examination, the neat CS-Alg fibers failed to present any

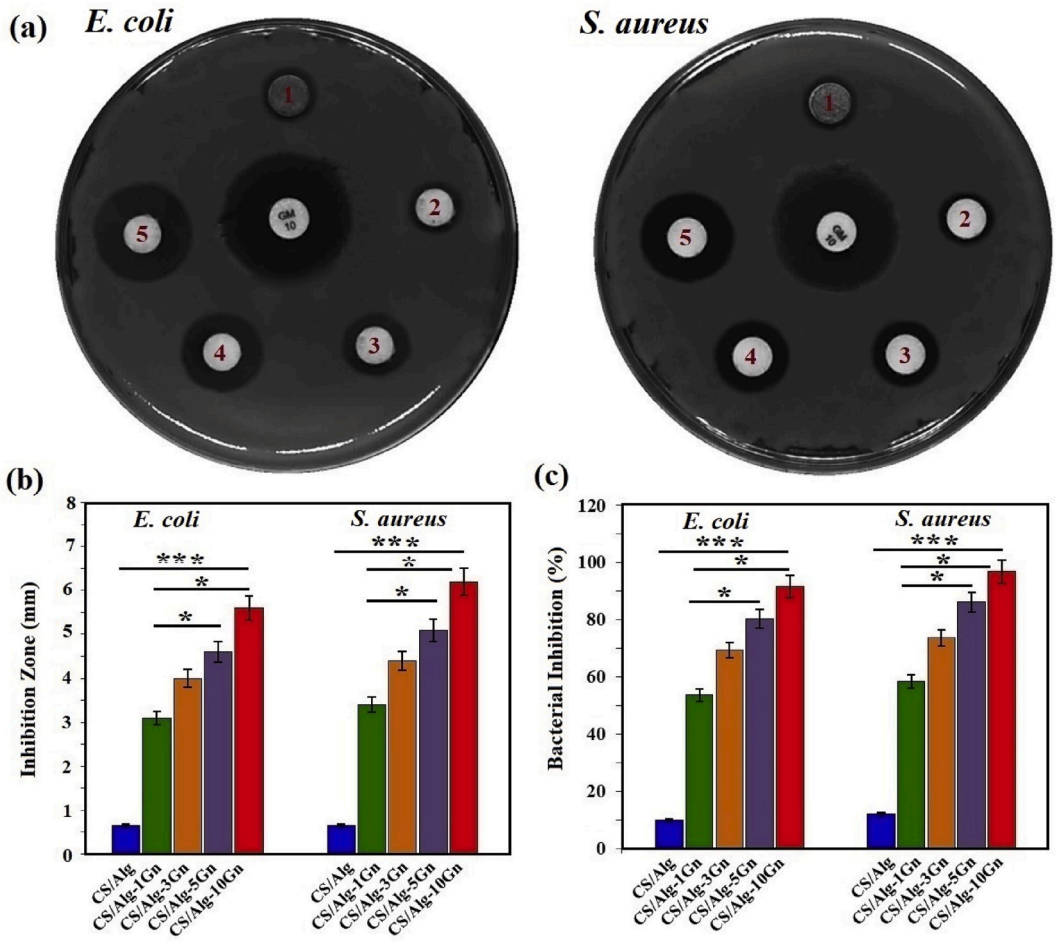

Fig. 6. (a) Inhibition zone images, (b) inhibition zone size, and (c) percent bacterial inhibition against *E. coli* and *S. aureus* for CS/Alg-Gn nanofibers with various Gn concentrations. Note in (a): (1) CS/Alg, (2) CS/Alg-1Gn, (3) CS/Alg-3Gn, (4) CS/Alg-5Gn, and (5) CS/Alg-10Gn. (*p < 0.05, ***p < 0.001).

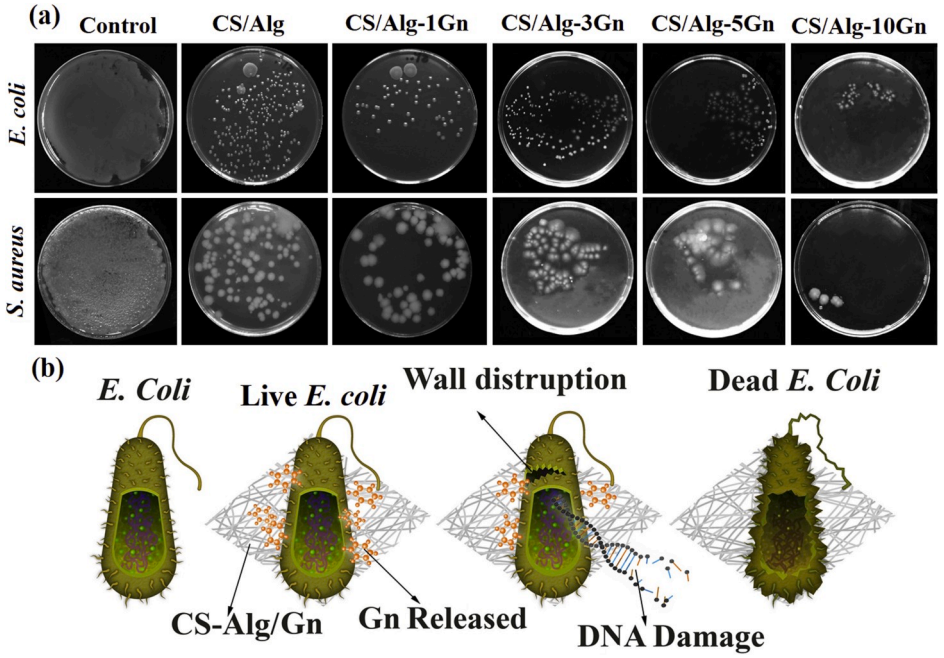

Fig. 7. (a) Images of CFUs of *E. coli* and *S. aureus* on CS/Alg-Gn nanofibers with various gentamicin concentrations and (b) schematic illustration of the antimicrobial mechanism of the nanofibers containing gentamicin.

antimicrobial performance towards bacteria. The CS-Alg/10Gn demonstrated the highest bacterial inhibition of 92.21 and 95.13% after 48 h incubation towards *S. aureus* and *E. coli*, respectively. In addition, an examination of colony forming units (CFUs) shows that CS-Alg scaffolds without Gn have no effect whereas CS-Alg scaffolds loaded with Gn drastically reduce the number of bacterial colonies (Fig. 7a). The number of CFUs decreases with increasing Gn concentration. All results verify that CS-Alg-xGn nanofibrous mats have the potential to prevent infection by both Gram-positive and Gram-negative bacteria. The mechanism of anti-bacterial activity of Gn is illustrated in Fig. 7b, wherein Gn kills bacteria by inhibiting protein formation, nucleic acid reproduction, formation of vital metabolites, and DNA destruction [58]. The interaction between Gn and bacterial cell walls results in cell membrane rupture and subsequent loss of cell functions.

3.5. In vivo study

Fig. 8a shows macroscopic photos of wounds from the different treatment groups along with wound contraction percentage measured 4 and 7 d post-injury. CS-Alg/3Gn nanofibers were selected for these in vivo experiments due to their superior performance in in vitro tests in terms of cytocompatibility and anti-bacterial properties, with their wound healing efficiency compared with plain CS-Alg and gauze groups. At day 4 post-injury, CS-Alg and CS-Alg/3Gn mats led to 18.49 ± 2.18 and 28.04 ± 1.71% wound closure, respectively; these values are significantly higher than the 13.81 ± 1.52% observed in the gauze-treated group ($p^* < 0.05$) (Fig. 8a). Furthermore, wound size significantly decreased by day 7 in the CS-Alg/3Gn and CS-Alg groups compared to the group treated with gauze. Specifically, wounds with nanofiber dressings containing Gn healed faster, with a wound contraction rate of 55.77 ± 2.3% after 7 d of treatment (Fig. 8b). All of the fabricated nanofibrous dressings adhered well to the surface of the burned area with no need for biological adhesives and could be easily peeled off without causing any injury to the wound site. This is attributed to the hydrophilic properties of the Alg and CS [3,5,45] that allowed the fabricated wound dressings to keep the wounds hydrated. A histological analysis was conducted to assess the healing progress of wounds from the three treatment groups on day 7 post-injury (Fig. 9a and b). The H&E images show that both the CS-Alg- and gauze-treated groups have obviously damaged dermal tissue with epidermal detachment and a high level of inflammatory cells including infiltration of macrophages within the tissue. Furthermore, no obvious epithelialization and epidermis regeneration is evident in the gauze-treated groups. However, the burn wounds treated with CS-Alg/3Gn nanofibers developed an epidermis layer with the formation of more skin appendages, including blood vessels, hair follicles, and sebaceous glands, and had less inflammatory cell infiltration than the other treatment groups. The gauze- and CS-Alg-treated groups display no complete formation of hair follicles or sebaceous glands.

To further evaluate the functionality of the nanofibers in wound healing progress, we stained wounds on day 7 with MT to assess collagen formation during skin regeneration, as wound healing is mainly dependent on collagen formation [59]. Fig. 9b clearly shows more collagen formation in the CS-Alg/3Gn-treated group compared to the gauze and CS-Alg groups. Specifically, denser collagen fibers in the form of well-arranged bundles are evident in the CS-Alg/3Gn group, while the gauze treated CS-Alg group displayed loose fibers and the smallest quantity of collagen fibers among all groups. Overall, the CS-Alg/3Gn wound dressing appears to advance the wound healing process in a short time. The CS-Alg/3Gn scaffold is hypothesized to disrupt the function of the cell membrane and then restrict nucleic acid synthesis by bacteria. In this regard, Gn within the CS-Alg interacts with the outer cell membrane of the bacteria leading to disruption of the cell membrane. Specifically, Gn is released from CS-Alg and attaches to the bacterial cell membrane, penetrating from the outer to inner membrane and leading to DNA damage [60]; this instantly introduces the drug into the bacteria, increasing the drug release rate. Ultimately, reducing the number of bacteria with the Gn released from the CS-Alg fibers would serve to keep the wound sterile and reduce the inflammatory responses, both of which help the wound to heal faster [61].

4. Conclusion

Gentamicin (Gn)-loaded chitosan-alginate (CS-Alg) scaffolds were fabricated via electrospinning to facilitate skin regeneration. The nanofibrous scaffolds had a porous and interconnected morphology featuring bead-free and randomly aligned continuous nanofibers. Increasing the Gn content from 1 to 5 wt% led to increased water uptake, mechanical strength, and deformation resistance, whereas further Gn addition reduced mechanical properties. The nanocomposite Gn-loaded CS-Alg scaffolds possessed antibacterial activity towards both Gram-negative and Gram-positive bacteria and were able to protect wounds from infection. MTT assays showed that cell survival on neat CS-Alg and CS-Alg/Gn mats with lower amounts of Gn was greater than on those with higher Gn amounts, implying a dose-related cytotoxicity with increasing Gn concentration. SEM images likewise indicated good cell

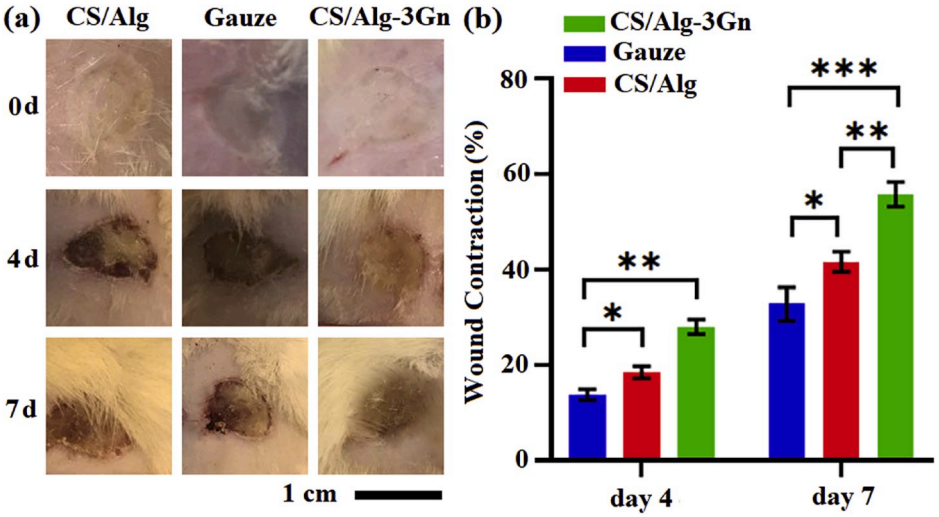

Fig. 8. Wound closure study: (a) macroscopic pictures of wounds treated with gauze, CS/Alg, or CS/Alg-3Gn at 7 d post-injury and (b) wound contraction rate as a function of time ($p^* < 0.05$, $p^{**} < 0.01$, $^{***}p < 0.001$).

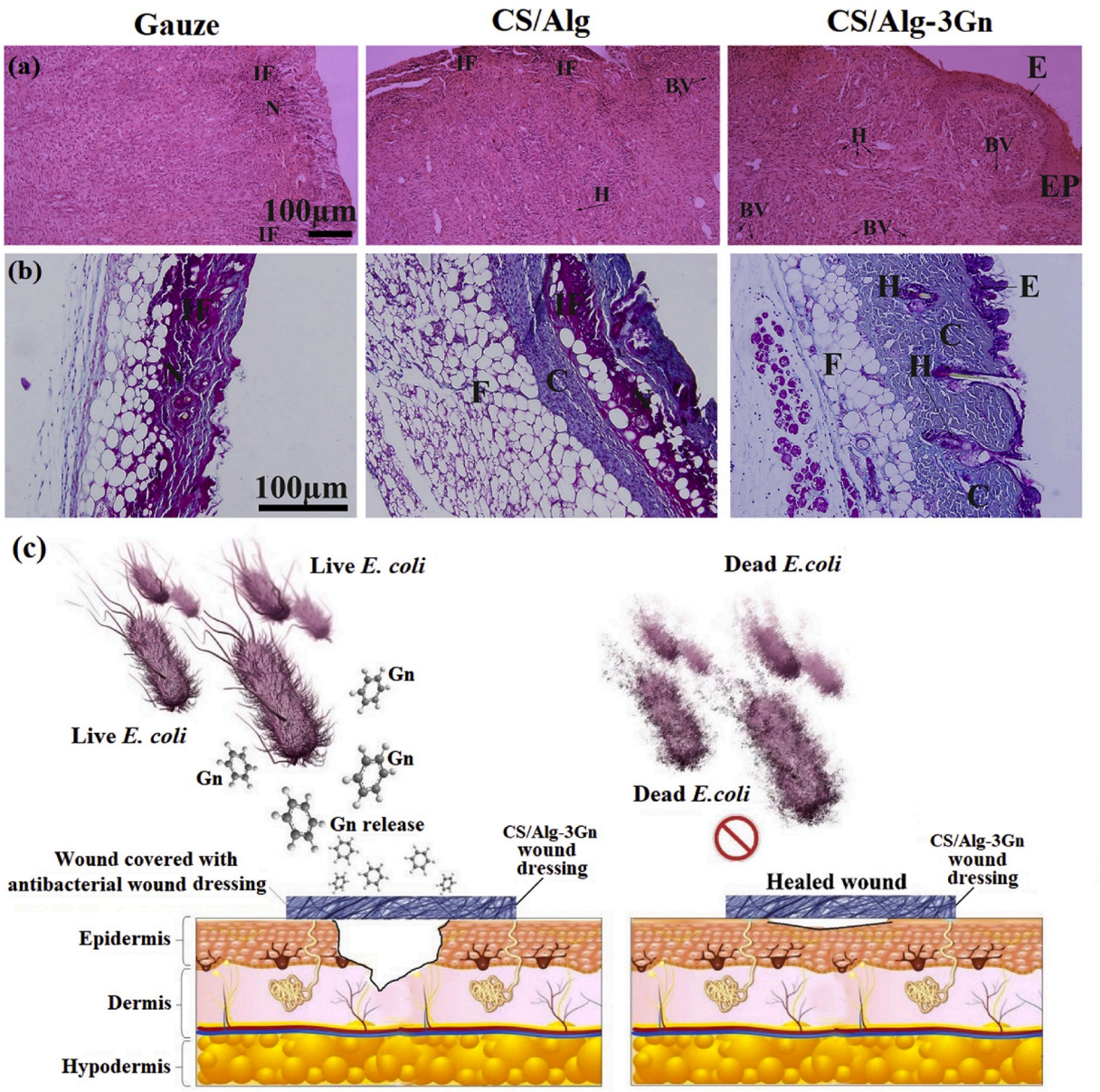

Fig. 9. Histopathological analysis: images of (a) H&E and (b) MT stained wounds treated with gauze, CS/Alg, or CS/Alg-3Gn dressings, and (c) schematic illustration of the wound healing process in the presence of a CS/Alg-Gn nanofiber scaffold (H: hair follicle, IF: inflammatory cells, N: necrotic tissue, BV: blood vessels, E: regenerated epidermis, EP: epithelialization, C: collagen, F: fatty cells).

attachment in the presence of low concentrations of the antibacterial agent. Furthermore, animal studies indicated that burn wounds treated with CS-Alg scaffolds with 3 wt% Gn healed more rapidly compared to those treated with scaffolds with a higher or lower Gn concentration owing to greater re-epithelialization, dense collagen formation, and development of blood vessels, hair follicles, and sebaceous glands. Overall, the results suggest the CS-Alg/3Gn wound dressing has great potential in applications such as treating burn wounds.

Declaration of competing interest

The authors declare that they have no known competing financial interests or personal relationships that could have appeared to influence the work reported in this paper.

CRediT authorship contribution statement

H.R. Bakhsheshi-Rad: Conceptualization, Supervision, Data curation, Writing - original draft, Formal analysis, Writing - review & editing. **Z. Hadisi:** Conceptualization, Methodology, Data curation, Writing - original draft, Formal analysis. **A.F. Ismail:** Supervision, Visualization, Writing - review & editing. **M. Aziz:** Supervision, Visualization, Writing - review & editing. **M. Akbari:** Supervision, Visualization, Writing - review & editing. **F. Berto:** Supervision, Visualization, Writing - review & editing. **X.B. Chen:** Supervision, Visualization, Writing - review & editing.

Acknowledgments

The authors acknowledge financial support from the Natural Sciences and Engineering Research Council (NSERC) of Canada, the Saskatchewan Health Research Foundation (SHRF), and Universiti Teknologi Malaysia (UTM).

Appendix A. Supplementary data

Supplementary data to this article can be found online at https://doi.org/10.1016/j.polymertesting.2019.106298.

References

[1] S. Gilotra, D. Chouhan, N. Bhardwaj, S.K. Nandi, B.B. Mandal, Potential of silk sericin based nanofibrous mats for wound dressing applications, Mater. Sci. Eng. C 90 (2018) 420–432.

[2] V.V.S.R. Karri, G. Kuppusamy, S.V. Talluri, S.S. Mannemala, R. Kollipara, A. D. Wadhwani, S. Mulukutla, K.R.S. Raju, R. Malayandi, Curcumin loaded chitosan nanoparticles impregnated into collagen-alginate scaffolds for diabetic wound healing, Int. J. Biol. Macromol. 93 (2016) 1519–1529.

[3] H. Xie, X. Chen, X. Shen, Y. He, W. Chen, Q. Luo, W. Ge, W. Yuan, X. Tang, D. Hou, D. Jiang, Q. Wang, Y. Liu, Q. Liu, K. Li, Preparation of chitosan-collagen-alginate composite dressing and its promoting effects on wound healing, Int. J. Biol. Macromol. 107 (2018) 93–104.

[4] H. Kaygusuz, E. Torlak, G. Akın-Evingür, İ. Özen, R. von Klitzing, F.B. Erim, Antimicrobial cerium ion-chitosan crosslinked alginate biopolymer films: a novel and potential wound dressing, Int. J. Biol. Macromol. 105 (2017) 1161–1165.

[5] R.L. Andersson, V. Ström, U.W. Gedde, P.E. Mallon, M.S. Hedenqvist, R.T. Olsson, Micromechanics of ultra-toughened electrospun PMMA/PEO fibres as revealed by in-situ tensile testing in an electron microscope, Sci. Rep. 4 (2014) 6335.

[6] H. Ren, Y. Cui, A. Li, D. Qiu, Bioactive glass sol as a dual function additive for chitosan-alginate hybrid scaffold, Chin. Chem. Lett. 29 (2018) 395–398.

[7] Z. Yin, J. Cao, Z. Li, D. Qiu, Reducing the bioavailability of cadmium in contaminated soil by dithiocarbamate chitosan as a new remediation, Environ. Sci. Pollut. Res. 22 (2015) 9668–9675.

[8] A. Mohandas, S. Deepthi, R. Biswas, R. Jayakumar, Chitosan based metallic nanocomposite scaffolds as antimicrobial wound dressings, Bioact. Mater. 3 (2018) 267–277.

[9] I. Olabarrieta, A. Jansson, U.W. Gedde, M.S. Hedenqvist, Mechanical and Physical properties of chitosan and whey blended with poly(ε-caprolactone), Int. J. Polym. Mater. 51 (2002) 275–289.

[10] F. Chen, M. Gällstedt, R.T. Olsson, U.W. Gedde, M.S. Hedenqvist, Unusual effects of monocarboxylic acids on the structure and on the transport and mechanical properties of chitosan films, Carbohydr. Polym. 132 (2015) 419–429.

[11] H.R. Bakhsheshi-Rad, M. Akbari, A.F. Ismail, et al., Coating biodegradable magnesium alloys with electrospun poly-L-lactic acid-åkermanite-doxycycline nanofibers for enhanced biocompatibility, antibacterial activity, and corrosion resistance, Surf. Coat. Technol. 377 (2019) 124898.

[12] R. Huang, W. Li, X. Lv, Z. Lei, Y. Bian, H. Deng, H. Wang, J. Li, X. Li, Biomimetic LBL structured nanofibrous matrices assembled by chitosan/collagen for promoting wound healing, Biomaterials 53 (2015) 58–75.

[13] H. Tu, G. Wu, Y. Yi, M. Huang, R. Liu, X. Shi, H. Deng, Layer-by-layer immobilization of amphoteric carboxymethyl chitosan onto biocompatible silk fibroin nanofibrous mats, Carbohydr. Polym. 210 (2019) 9–16.

[14] S. Xin, X. Li, Q. Wang, R. Huang, X. Xu, Z. Lei, H. Deng, Novel layer-by-layer structured nanofibrous mats coated by protein films for dermal regeneration, J. Biomed. Nanotechnol. 10 (2014) 803–810.

[15] S. Jiang, J. Lv, M. Ding, Y. Li, H. Wang, S. Jiang, Release behavior of tetracycline hydrochloride loaded chitosan/poly(lactic acid) antimicrobial nanofibrous membranes, Mater. Sci. Eng. C 59 (2016) 86–91.

[16] I. Olabarrieta, D. Forsström, U.W. Gedde, M.S. Hedenqvist, Transport properties of chitosan and whey blended with poly(ε-caprolactone) assessed by standard permeability measurements and microcalorimetry, Polymer 42 (2001) 4401–4408.

[17] I. Olabarrieta, D. Forsström, U.W. Gedde, M.S. Hedenqvist, Transport properties of chitosan and whey blended with poly(ε-caprolactone) assessed by standard permeability measurements and microcalorimetry, Polymer 42 (2001) 4401–4408.

[18] F. Chen, X. Monnier, M. Gällstedt, U.W. Gedde, M.S. Hedenqvist, Wheat gluten/chitosan blends: a new biobased material, Eur. Polym. J. 60 (2014) 186–197.

[19] L. Xing, Y. Ma, H. Tan, G. Yuan, S. Li, J. Li, Y. Jia, T. Zhou, X. Niu, X. Hu, Alginate membrane dressing toughened by chitosan floccule to load antibacterial drugs for wound healing, Polym. Test. 79 (2019) 106039.

[20] F. Chen, M. Gällstedt, R.T. Olsson, U.W. Gedde, M.S. Hedenqvist, A novel chitosan/wheat gluten biofoam fabricated by spontaneous mixing and vacuum-drying, RSC Adv. 5 (2015) 94191–94200.

[21] B. Kaczmarek, A. Sionkowska, J. Stojkovska, Characterization of scaffolds based on chitosan and collagen with glycosaminoglycans and sodium alginate addition, Polym. Test. 68 (2018) 229–232.

[22] H.R. Bakhsheshi-Rad, A.F. Ismail, M. Aziz, Z. Hadisi, M. Omidi, X. Chen, Antibacterial activity and corrosion resistance of Ta_2O_5 thin film and electrospun PCL/MgO-Ag nanofiber coatings on biodegradable Mg alloy implants, Ceram. Int. 45 (2019) 11883–11892.

[23] H.R. Bakhsheshi-Rad, Z. Hadisi, E. Hamzah, et al., Drug delivery and cytocompatibility of ciprofloxacin loaded gelatin nanofibers-coated Mg alloy, Mater. Lett. 207 (2017) 179–182.

[24] X. Lv, W. Zhang, Y. Liu, Y. Zhao, J. Zhang, M. Hou, Hygroscopicity modulation of hydrogels based on carboxymethyl chitosan/Alginate polyelectrolyte complexes and its application as pH-sensitive delivery system, Carbohydr. Polym. 198 (2018) 86–93.

[25] S. Kondaveeti, P.V.d.A. Bueno, A.M. Carmona-Ribeiro, F. Esposito, N. Lincopan, M. R. Sierakowski, D.F.S. Petri, Microbicidal gentamicin-alginate hydrogels, Carbohydr. Polym. 186 (2018) 159–167.

[26] G. Tao, Y. Wang, R. Cai, H. Chang, K. Song, H. Zuo, P. Zhao, Q. Xia, H. He, Design and performance of sericin/poly(vinyl alcohol) hydrogel as a drug delivery carrier for potential wound dressing application, Mater. Sci. Eng. C 101 (2019) 341–351.

[27] J.-S. Deng, L. Li, D. Stephens, Y. Tian, F.W. Harris, S.Z.D. Cheng, Effect of γ-radiation on a polyanhydride implant containing gentamicin sulfate, Int. J. Pharm. 232 (2002) 1–10.

[28] S.K. Jaganathan, M. Prasath Mani, M. Ayyar, R. Rathanasamy, Biomimetic electrospun polyurethane matrix composites with tailor made properties for bone tissue engineering scaffolds, Polym. Test. 78 (2019) 105955.

[29] Ł. Rumian, H. Tiainen, U. Cibor, M. Krok-Borkowicz, M. Brzychczy-Włoch, H. J. Haugen, E. Pamuła, Ceramic scaffolds enriched with gentamicin loaded poly (lactide-co-glycolide) microparticles for prevention and treatment of bone tissue infections, Mater. Sci. Eng. C 69 (2016) 856–864.

[30] M. Parent, A. Magnaudeix, S. Delebassée, E. Sarre, E. Champion, M. Viana Trecant, C. Damia, Hydroxyapatite microporous bioceramics as vancomycin reservoir: antibacterial efficiency and biocompatibility investigation, J. Biomater. Appl. 31 (2016) 488–498.

[31] Ł. Rumian, H. Tiainen, U. Cibor, M. Krok-Borkowicz, M. Brzychczy-Włoch, H. J. Haugen, E. Pamuła, Ceramic scaffolds with immobilized vancomycin-loaded poly(lactide-co-glycolide) microparticles for bone defects treatment, Mater. Lett. 190 (2017) 67–70.

[32] M.Q. Khan, D. Kharaghani, Sanaullah, A. Shahzad, Y. Saito, T. Yamamoto, H. Ogasawara, I.S. Kim, Fabrication of antibacterial electrospun cellulose acetate/silver-sulfadiazine nanofibers composites for wound dressings applications, Polym. Test. 74 (2019) 39–44.

[33] B. Wang, Z. Ye, Q. Xu, L. Sun, Y. Wang, S. Shi, Z. Wang, X. Xu, J. Qu, K. Nan, In situ construction of Ag NPs in bio-inspired multilayer films for long-term bactericidal and biofilm inhibition properties, Polym. Test. 62 (2017) 162–170.

[34] D. Kharaghani, M.Q. Khan, Y. Tamada, H. Ogasawara, Y. Inoue, Y. Saito, M. Hashmi, I.S. Kim, Fabrication of electrospun antibacterial PVA/Cs nanofibers loaded with CuNPs and AgNPs by an in-situ method, Polym. Test. 72 (2018) 315–321.

[35] R. Alipour, A. Khorshidi, A.F. Shojaei, F. Mashayekhi, M.J.M. Moghaddam, Skin wound healing acceleration by Ag nanoparticles embedded in PVA/PVP/Pectin/Mafenide acetate composite nanofibers, Polym. Test. 79 (2019) 106022.

[36] J. Pant, J S, M.J. Goudie, D.T. Nguyen, H. Handa, Antibacterial 3D bone scaffolds for tissue engineering application, J. Biomed. Mater. Res. B 107 (2019) 1068–1078.

[37] P. Karuppuswamy, J.R. Venugopal, B. Navaneethan, A.L. Laiva, S. Ramakrishna, Polycaprolactone nanofibers for the controlled release of tetracycline hydrochloride, Mater. Lett. 141 (2015) 180–186.

[38] A. Rapacz-Kmita, M.M. Bućko, E. Stodolak-Zych, M. Mikołajczyk, P. Dudek, M. Trybus, Characterisation, in vitro release study, and antibacterial activity of montmorillonite-gentamicin complex material, Mater. Sci. Eng. C 70 (2017) 471–478.

[39] H.R. Bakhsheshi-Rad, X.B. Chen, A.F. Ismail, et al., Improved antibacterial properties of an Mg-Zn-Ca alloy coated with chitosan nanofibers incorporating silver sulfadiazine multiwall carbon nanotubes for bone implants, Polym. Adv. Technol. 30 (2019) 1333–1339.

[40] H.R. Bakhsheshi-Rad, E. Hamzah, M.K. Asgarani, et al., Deposition of nanostructured fluorine-doped hydroxyapatite–polycaprolactone duplex coating to enhance the mechanical properties and corrosion resistance of Mg alloy for biomedical applications, Mater. Sci. Eng. C 60 (2016) 526–537.

[41] H. Hou, J.J. Ge, J. Zeng, Q. Li, D.H. Reneker, A. Greiner, S.Z.D. Cheng, Electrospun polyacrylonitrile nanofibers containing a high concentration of well-aligned multiwall carbon nanotubes, Chem. Mater. 17 (2005) 967–973.

[42] D. Papkov, Y. Zou, M.N. Andalib, A. Goponenko, S.Z.D. Cheng, Y.A. Dzenis, Simultaneously strong and tough ultrafine continuous nanofibers, ACS Nano 7 (2013) 3324–3331.

[43] P. Wang, C.N. Moorefield, K.-U. Jeong, S.-H. Hwang, S. Li, S.Z.D. Cheng, G. R. Newkome, Dendrimer–metallomacrocycle composites: nanofiber formation by multi-ion pairing, Adv. Mater. 20 (2008) 1381–1385.

[44] J.J. Ge, H. Hou, Q. Li, M.J. Graham, A. Greiner, D.H. Reneker, F.W. Harris, S.Z. D. Cheng, Assembly of well-aligned multiwalled carbon nanotubes in confined polyacrylonitrile environments: Electrospun composite nanofiber sheets, J. Am. Chem. Soc. 126 (2004) 15754–15761.

[45] C. Flores, M. Lopez, N. Tabary, C. Neut, F. Chai, D. Betbeder, C. Herkt, F. Cazaux, V. Gaucher, B. Martel, N. Blanchemain, Preparation and characterization of novel chitosan and β-cyclodextrin polymer sponges for wound dressing applications, Carbohydr. Polym. 173 (2017) 535–546.

[46] H. Adeli, M.T. Khorasani, M. Parvazinia, Wound dressing based on electrospun PVA/chitosan/starch nanofibrous mats: fabrication, antibacterial and cytocompatibility evaluation and in vitro healing assay, Int. J. Biol. Macromol. 122 (2019) 238–254.

[47] S. Agarwal, J.H. Wendorff, A. Greiner, Use of electrospinning technique for biomedical applications, Polymer 49 (2008) 5603–5621.

[48] H.R. Bakhsheshi-Rad, X.B. Chen, A.F. Ismail, M. Aziz, E. Hamzah, A. Najafinezhad, A new multifunctional monticellite-ciprofloxacin scaffold: preparation, bioactivity, biocompatibility, and antibacterial properties, Mater. Chem. Phys. 222 (2019) 118–131.

[49] H.R. Bakhsheshi-Rad, A.F. Ismail, M. Aziz, M. Akbari, Z. Hadisi, M. Daroonparvar, X.B. Chen, Antibacterial activity and in vivo wound healing evaluation of polycaprolactone-gelatin methacryloyl-cephalexin electrospun nanofibrous, Mater. Lett. 256 (2019) 126618.

[50] C. Gandhimathi, J.R. Venugopal, V. Bhaarathy, S. Ramakrishna, S.D. Kumar, Biocomposite nanofibrous strategies for the controlled release of biomolecules for skin tissue regeneration, Int. J. Nanomed. 9 (2014) 4709.
[51] C.D. Johnson, A.R. D'Amato, R.J. Gilbert, Electrospun fibers for drug delivery after spinal cord injury and the effects of drug incorporation on fiber properties, Cells Tissues Organs 202 (2016) 116–135.
[52] P. Parsa, A. Paydayesh, S.M. Davachi, Investigating the effect of tetracycline addition on nanocomposite hydrogels based on polyvinyl alcohol and chitosan nanoparticles for specific medical applications, Int. J. Biol. Macromol. 121 (2019) 1061–1069.
[53] S. Hasatsri, A. Pitiratanaworanat, S. Swangwit, C. Boochakul, C. Tragoonsupachai, Comparison of the morphological and physical properties of different absorbent wound dressings, Dermatol. Res. Pract. 2018 (2018) 6.
[54] H. Matsumoto, A. Tanioka, Functionality in electrospun nanofibrous membranes based on fiber's size, surface area, and molecular orientation, Membranes 1 (2011) 249–264.
[55] S. Soliman, S. Sant, J.W. Nichol, M. Khabiry, E. Traversa, A. Khademhosseini, Controlling the porosity of fibrous scaffolds by modulating the fiber diameter and packing density, J. Biomed. Mater. Res. A 96 (2011) 566–574.
[56] Y. Liu, S. Zhou, Y. Gao, Y. Zhai, Electrospun nanofibers as a wound dressing for treating diabetic foot ulcer, Asian J. Pharm. Sci. 14 (2019) 130–143.
[57] G. Jin, M.P. Prabhakaran, D. Kai, M. Kotaki, S. Ramakrishna, Electrospun photosensitive nanofibers: potential for photocurrent therapy in skin regeneration, Photochem. Photobiol. Sci. 12 (2013) 124–134.
[58] A.I. Barzic, S. Ioan, Antibacterial Drugs—From Basic Concepts to Complex Therapeutic Mechanisms of Polymer Systems, Concepts, Compounds and the Alternatives of Antibacterials, Varaprasad Bobbarala, vol. 2015, IntechOpen, 2015.
[59] C.-w. Li, Q. Wang, J. Li, M. Hu, S.-j. Shi, Z.-w. Li, G.-l. Wu, H.-h. Cui, Y.-y. Li, Q. Zhang, Silver nanoparticles/chitosan oligosaccharide/poly (vinyl alcohol) nanofiber promotes wound healing by activating TGFβ1/Smad signaling pathway, Int. J. Nanomed. 11 (2016) 373.
[60] M.A. Elfaky, A.K. Thabit, A. Sirwi, U.A. Fahmy, et al., Development of a novel pharmaceutical formula of nanoparticle lipid carriers of gentamicin/α-tocopherol and in vivo assessment of the antioxidant protective effect of α-tocopherol in gentamicin-induced nephrotoxicity, Antibiotics 8 (2019) 234.
[61] O. Sarheed, A. Ahmed, D. Shouqair, J. Boateng, Antimicrobial dressings for improving wound healing, in: V. Alexandrescu (Ed.), Wound Healing-New Insights into Ancient Challenges, 2016, pp. 373–398.